Royal Netherlands Meteorological Institute
Ministry of Infrastructure and the Environment

The EUMETSAT Network of Satellite Application Facilities

OSI SAF
Ocean and Sea Ice

EUMETSAT

Ocean and Sea Ice SAF

Technical Note
SAF/OSI/KNMI/TEC/TN/163

Calibration and Validation of ASCAT Winds

Jeroen Verspeek
Marcos Portabella
Ad Stoffelen
Anton Verhoef

Version 5.1

May 2013

DOCUMENTATION CHANGE RECORD

Reference: SAF/OSI/KNMI/TEC/TN/163

Issue / Revision :	Date :	Change :	Description :
Version 0.9	2007-02-22		Draft version.
Version 1.0	2007-06-15	Major	Adapted description and figures Adapted correction tables and monitoring tables
Version 2.0	2007-10-01	Major	Adapted document to one-transponder calibrated data
Version 2.1	2007-10-22	Minor	Title changed, minor adaptations
Version 3.0	2008-03-26	Major	Adapted document to three-transponder calibrated data
Version 3.1	2008-10-01	Minor	Added section about MLE normalisation. Adaptations on figures and tables
Version 4.0	2008-11-25	Major	Adapted document to L1b version PPF6.3.0.
Version 4.1	2009-05-12	Minor	Adapted references.
Version 5.0	2011-06-24	Major	Adapted document to L1b version PPF7.4.0 and to NOC corrections.
Version 5.1	2013-05-30	Minor	Added comment on Bayesian ice screening method.

Summary

Based on the OSI SAF cone visualisation tools at KNMI and the NOC corrections, calibration of the ASCAT scatterometer is checked. In this report we describe and evaluate level 1b corrections to the operational L1b ASCAT backscatter data version PPF740 as provided by EUMETSAT based on their three transponder calibration campaign. For the left mid antenna an offset in ocean calibration results has disappeared with respect to the former version, suggesting improved L1b calibration as anticipated. For all antennas the “wiggles” have reduced in amplitude. In the outer swath consistent large departures remain, which may be included in an updated version of the geophysical model function, i.e., CMOD5na. Indeed, still the ASCAT wind product based on L1b version PPF740 shows very similar characteristics to the ASCAT scatterometer wind product based on L1b version PPF730 and meets the wind product requirements.

Deviations between scatterometer and Numerical Weather Prediction wind derived backscatter still show a significant improvement after correction. Without correction the difference ranges from +0.4 dB to -0.8 dB going from the inner side to the outer side of the swaths. Also, the PPF 740 L1b data show smaller interbeam differences and the wiggles in the antennas have been reduced. After the NOC correction is applied the difference ranges from -0.12 dB to +0.26 dB and is almost identical for the PPF740 and the PPF730 L1b data.

The operational OSI SAF ASCAT level 2 wind product stream runs at KNMI using the validated ASCAT level 1b stream at 12.5 km and 25 km sampling as input, and may be maintained without any significant effects on product quality. The new L1b σ^0 stream will be corrected using the new linear scaling factors in the transformed z domain, which correspond to addition factors in the logarithmic domain (dB). These changes correspond to slightly resetting the ASCAT instrument gain per beam and per Wind Vector Cell (WVC) in order to maintain the backscatter data consistency and wind product quality.

Contents

1 Introduction

An operational OSI SAF ASCAT level 2 wind product stream is running at KNMI using the commissioning ASCAT L1b stream at 12.5 and 25 km sampling as input. The L1b σ^0 stream is corrected using linear scaling factors in the transformed z domain [STOFFELEN and ANDERSON 1997], corresponding to addition factors in the logarithmic domain (dB). These changes correspond to resetting the ASCAT instrument gain per beam and per Wind Vector Cell (WVC). The objective is set to reproduce wind distributions similar to those from the ERS scatterometer, which provides a transfer standard from the ERS to the ASCAT era.

The Advanced Scatterometer (ASCAT) [FIGA et al 2002] is part of the payload of the MetOp satellite series of which the first one, MetOp-A, has been successfully launched on 19 October 2006. ASCAT is a fan beam scatterometer with six fan beam antennae providing a swath of WVCs both to the left and right of the satellite subsatellite track. Each swath is thus illuminated by three beams and is divided into 41 WVCs of 12.5 km size, numbered from 1-82 from left to right across both swaths (when looking into the satellite propagation direction. [STOFFELEN and ANDERSON 1997] describe the so-called measurement space. In this space the three backscatter measurements are plotted along three axis, spanning the fore, mid and aft beam backscatter measurements. As the satellite propagates and the wind conditions on the ocean surface vary in each numbered WVC, the 3D measurement space will be filled. CMOD5 [HERSBACH 2007] describes the geophysical dependency of the backscatter measurements on the WVC-mean wind vector as derived from ERS scatterometer data. Since, this dependency involved two geophysical parameters, namely two orthogonal wind components (or wind speed and direction), the 3D measurement space is filled with measurements closely following a 2D surface [STOFFELEN and ANDERSON 1997]. This folded surface is conical and consists of two sheets, one sheet for when the wind vector blows against the mid beam pointing direction (upwind section) and one for an along mid beam pointing direction wind vector (downwind section). The knowledge on the position of this surface through the Geophysical Model Function (GMF), CMOD5 provides a powerful diagnostic capability for the calibration and validation of the ASCAT scatterometer, since the same geophysical dependency should apply for both the ERS and MetOp scatterometers.

Besides ocean calibration EUMETSAT relies on the rain forest response, the backscatter over ice and transponder measurements for ASCAT calibration [FIGA et al 2004]. In this report we explore ocean calibration. In this report we assume that the main challenge lies in setting the antenna pattern or gain settings of the six beams and explore normalisation corrections to the experimental L1b backscatter data as provided by EUMETSAT during the commissioning phase of MetOp.

EUMETSAT has provided several preliminary datasets during the MetOp commissioning:

1) from 19 October 2006 until 29 January 2007, denoted “ss” data;
2) from 30 January 2007 until 12 February 2007, denoted as “zz” data;
3) from 13 February 2007 until 10 October 2007. (latest configuration of the pre-validated L1b data stream denoted as “zzz” data)
4) from 10 October 2007 until 28 February 2008. One-transponder calibrated data, denoted as “PPF530” data with reference to the level 1B processor software version. This data was previously denoted as “z4” data
5) from 28 February 2008 to 23 October 2008. Three-transponder calibrated data, denoted as “PPF550”.
6) from 23 October 2008 to 27 November 2008, “PPF620” data.
7) from 27 November 2008 to 7 September 2009, “PPF630” data
8) from 7 September 2009 to …July 2011, “PPF730” data
9) from …July 2011 onwards, “PPF740” data

A synchronized data set from L1b version PPF740 and PPF730 was provided by EUMETSAT, of which data from 2011-03-26 to 2011-04-10 is used in this document.

In this document these synchronized data sets are used. From March 2008 onwards the L1B software identifier is written in the BUFR message and is used for automatic determination of the applicable calibration correction table in the ASCAT Wind Data Processor (AWDP).

In section 2 and 3 the correction based on the NWP Ocean Calibration (NOC) residuals and the normalisation correction based on the averaged backscatter difference between the two level 1b software versions PPF740 and PPF730 are described respectively. Section 4 shows the data in measurement space as well as the total (NOC+normalisation) correction factors. In sections 5, 6 and 7 the ocean calibration results, the wind statistics, and the Maximum Likelihood Estimator (MLE) statistics are discussed, respectively. The conclusions and outlook are presented in section 8. Note that correction tables are listed in appendix A1 and A2.

In 2012, a Bayesian sea ice screening algorithm was introduced in the operational ASCAT wind processing. This algorithm replaces the ice screening based on the Sea Surface Temperature (SST) field from the ECMWF global NWP model. It was extensively tested that the new algorithm is better capable to distinguish between open water and sea ice, especially during melting and freezing. The ice screening algorithm is extensively described in [BELMONTE 2012]. The ice screening method does not change the results in this report, since it only influences the regions where winds will be available or not, near the ice edges; it does not influence the wind retrieval itself.

2 NOC correction

The NOC method resides in direct comparison of measured σ_0 data with simulated values from NWP winds using the GMF [Stoffelen, 1998; Freilich, 1999; Verspeek, 2011]. For the ASCAT and ERS scatterometers, the NOC estimates <z>, i.e. the mean transformed backscatter over the ocean for a uniform wind direction distribution and compares it with the mean measured backscatter over the ocean for a given wind distribution.

The NOC technique [Stoffelen 1998] is used to assess the difference between scatterometer backscatter data and simulated backscatter data out of collocated NWP winds using the GMF. Discrepancies between mean measured and simulated backscatter may be due to instrument calibration, systematic and random errors in NWP wind speed and direction and GMF errors. These sources of error should therefore be analyzed carefully. The NOC method is based on the analysis of a large measurement dataset to estimate Fourier coefficients that can be directly compared to those in the CMOD5.n GMF. For any particular WVC in any beam the incidence angle is very nearly constant around the orbit and we can model the backscatter with

$$\sigma_0(v,\phi) = B_0(v)[1 + B_1(v)\cos\phi + B_2(v)\cos(2\phi)]^{1.6}$$

where v is wind speed and ϕ is wind direction with respect to the beam pointing direction. The mean backscatter is essentially determined by the value of B_0 with contributions from B_1 and B_2. In z-space, where $z = \sigma_0^{0.625}$, this becomes

$$z(v,\phi) = \frac{1}{2}a_0(v) + a_1(v)\cos\phi + a_2(v)\cos(2\phi)$$

where $a_0 = 2B_0^{0.625}$, $a_1 = B_1B_0^{0.625}$ and $a_2 = B_2B_0^{0.625}$. Integrating uniformly over the azimuth angle gives

$$\frac{1}{2\pi}\int_0^{2\pi} z(v,\phi)\,d\phi = \frac{1}{2}a_0(v)$$

As such, when the wind direction distribution is sampled uniformly for all wind speeds, the mean of $2a_0$ should be identical to the mean of z. This means that uncertainties in a_1 and a_2 do not contribute to the error in the simulated mean z.

To arrange a uniform wind direction distribution, we split the data into wind speed bins and azimuth angle bins. Bins are defined so that they are large enough to contain a certain minimum number of measurements and small enough to provide a good approximation of the integral. In the following, indices i and j refer to wind speed bin i and azimuth angle bin j respectively. Index k is used to refer to an individual measurement z_k. Parameters I, J and K refer to the total number of bins or measurements, so $i=1, 2 ..., I,\ j=1, 2 ... ,J$ and $k=1, 2 ... ,K(i,j)$.

The mean z in a fixed wind speed row is, let's call this $z(i)$:

$$z(i) = \frac{1}{J} \sum_{j=1}^{J} \frac{1}{K(i,j)} \sum_{k=1}^{K(i,j)} z_k(i,j)$$

Summation over the wind speed rows gives

$$\langle z \rangle = \frac{1}{KJI} \sum_{i=1}^{I} KJ(i) z(i)$$

with

$$KJ(i) = \sum_{j=1}^{J} K(i,j), \quad KJI = \sum_{i=1}^{I} \sum_{j=1}^{J} K(i,j)$$

<z> is the mean backscatter value over a uniform wind direction distribution and may be either measured or simulated by collocated NWP wind inputs and the GMF, where mainly the term as given by $a_0(v)$ or $B_0(v)$ contributes. Any discrepancy between the simulated and measured mean backscatter values is computed as a ratio. A ratio not equal to one may be related to inaccuracies in the instrument gain, e.g., beam pattern determination, or to errors in the NWP input winds and GMF.

This method needs only a few days of collocated ASCAT data and ECMWF winds to produce a reasonable estimate of difference in a_0. We use CMOD5.n with the ECMWF equivalent neutral 10-meter winds to calculate model backscatter values corresponding to the collocated measured values and apply the process as described above. The difference between the two values of a_0 then provides an estimate of the mean difference between model and measurement backscatter.

The ocean calibration gives residuals in backscatter as a function of incidence angle for each antenna. When these residuals are stable over time they may be used as correction factors for errors in the instrument, for monitoring instrument health or for GMF development.

A time series of the ocean calibration is performed over the period of one year, from 2008-09-01 to 2009-08-31 for the ASCAT scatterometer in both 25 km and 12.5 km WVC spacing resolution. The one-year period is taken to average out the seasonal variations in the wind distribution that have an effect on the NOC residual. Successive periods of day 1-14 and day 15-last day of the month are taken as input for an ocean calibration run. The cone corrections [Verspeek et al, 2008] need not be applied anymore.

We use the OSI SAF visualisation package [VERSPEEK 2006-2] to produce visualisation plots in z-space, i.e., (z_{fore}, $z_{aft,}$ z_{mid}) where $z=(\sigma°)^{0.625}$ [STOFFELEN, 1998]. Figure 1 is an example of such a visualisation from ASCAT. The double cone surface of CMOD5n is depicted in blue. The measured data is shown as a cloud of black points around the cone surface. The cloud of ASCAT backscatter ($\sigma°$) triplets (corresponding to the fore, mid, and aft beams) match the CMOD5n GMF in the 3-D measurement space [HERSBACH 2007].

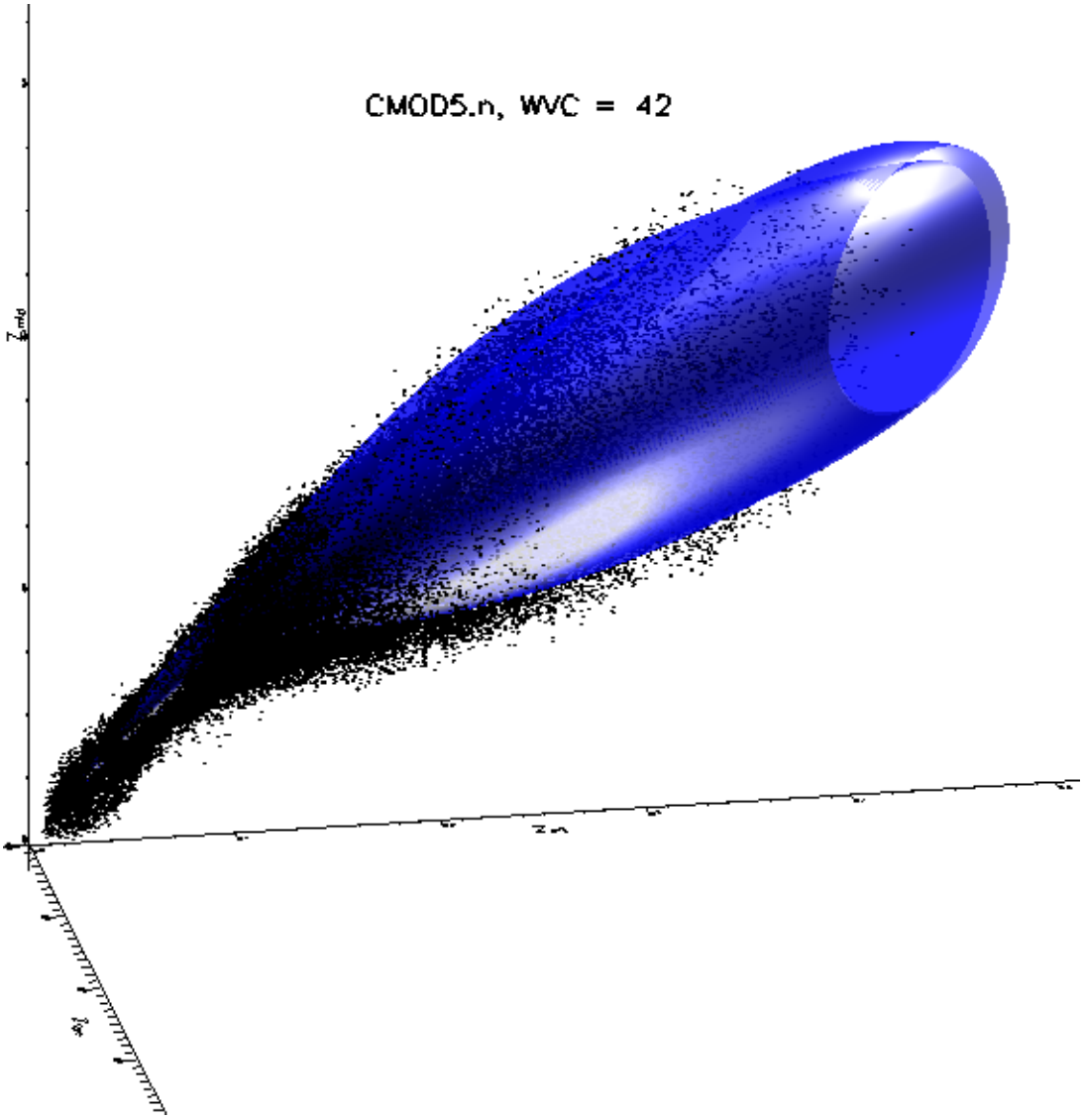

Figure 1 – CMOD5.n wind cone with measured data points for WVC 42, the innermost WVC of the right swath.

3 Normalisation correction

The NOC corrections were applied to adapt the backscatter values in the original (version 7.2) L1b stream with the 3-transponder calibrated data. Since the launch of METOP-A, EUMETSAT several times improved their normalisation tables in the L1b processing. A correction that accounts for the differences in level1B software processing versions is applied. These corrections have been able to transform the ASCAT backscatter measurements from each L1B calibration cycle to the next cycle within a few hundredths of a dB with L1B software version 7.2 taken as the reference. Thus the results are made independent of the level1B software version that is used.

The normalisation factors are assumed to be multiplication factors in linear space, like the visual correction that we apply. Because all correction factors are linear, the corrections can be applied on top of each other. Normalisation correction tables are determined for each update of the L1b data.

This is done by averaging the σ^0 differences in dB value from the new L1b data stream and the parallel original L1b data steam over one or more collocated orbits. The differences appear rather constant and show insignificant spread, confirming that the main effect in these conversions is a gain factor. Figure 2a) shows the average value per antenna and WVC of the difference in σ^0 value between the PPF740 and the PPF730 data stream. Figure 2b) shows the standard deviation (SD) for the correction as shown in Figure 2a). Figure 2c) and Figure 2d) show the same for the 25 km resolution product. Synchronized batches are used for an assessment of the spread in the differences (SD). The differences show a smooth course. The SD plot in Figure 2b) shows a systematic deviation for the mid beams with increasing SD going from the center of the swath toward the near swath and the far swath. This is caused by a wrong implementation of a table for the Hamming window width as a function of WVC in the level 1b processing which has been corrected for in the new version. This correction was only needed for the 12.5 km product so it is does not show up in the SD plot for the 25 km resolution in Figure 2d). For the other beams the SD plots show small values indicating that the pattern is persistent. It is an order of magnitude below the typical calibration changes. This is compatible with all earlier ASCAT calibration changes, thus guaranteeing a constant-quality backscatter input to the L2 processing.

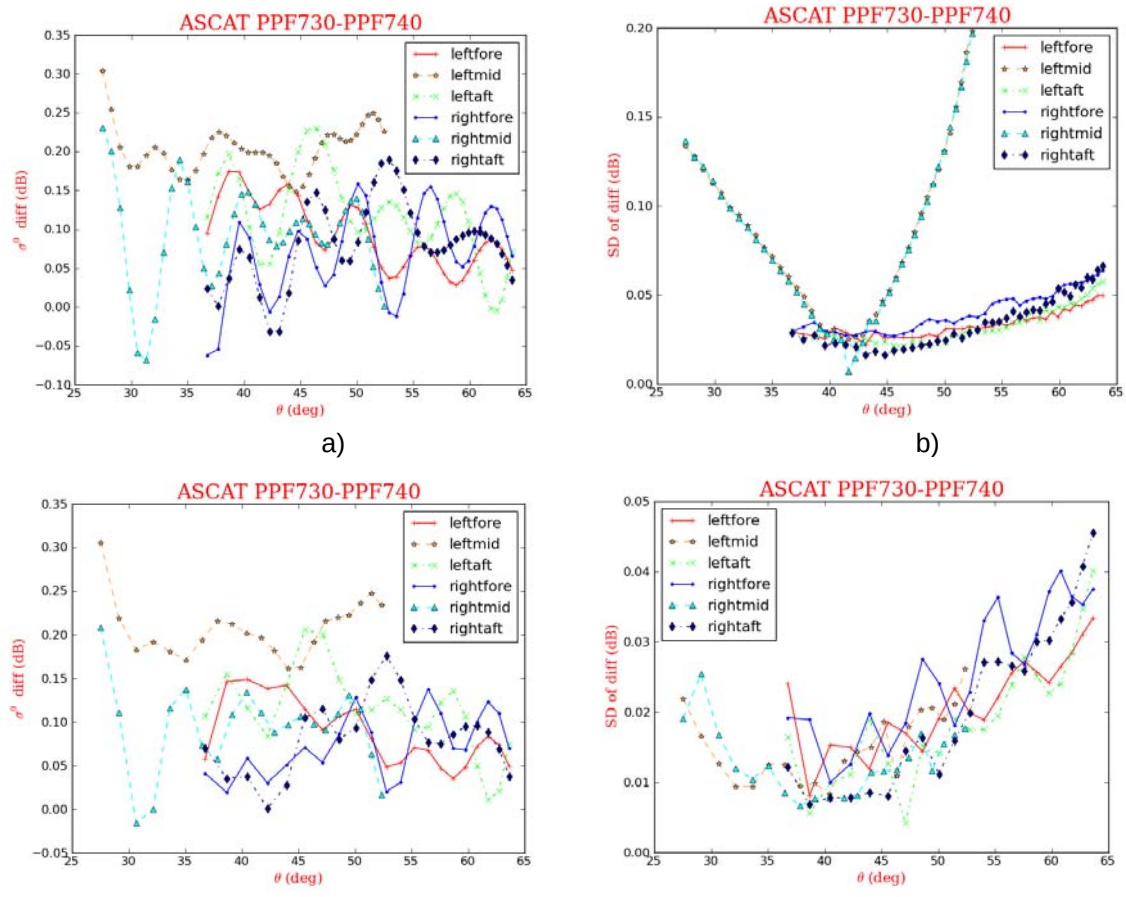

Figure 2 – Average and standard deviation of the difference between the L1b versions PPF740 and PPF730 for the fore, mid and aft antenna as a function of incidence angle.
a) average of σ^0 difference, 12.5 km resolution
b) standard deviation of the difference, 12.5 km resolution
c) average of σ^0 difference, 25 km resolution
d) standard deviation of the difference, 25 km resolution

Figure 3a) shows the backscatter difference for the fore antenna from the ascending part of the orbits on 2011-03-27. Any dependency of the difference in backscatter on geographical location should be visible in these figures. The dependency appears to be mainly on WVC number or incidence angle. The orbits have a systematic pattern across the swath, showing the WVC dependency of the correction. Figure 3b) shows the same data corrected for the average PPF740-

PPF730 σ^0 difference as shown in Figure 2a). The remaining difference is small and rather uniform, no pattern as function of incidence angle can be observed. Figure 3c) and Figure 3d) show the same for the mid beam. In Figure 3d) an increase in the remaining difference when going from the center of the swath to the outer sides can be seen. This is consistent with Figure 2b) and has the same cause.

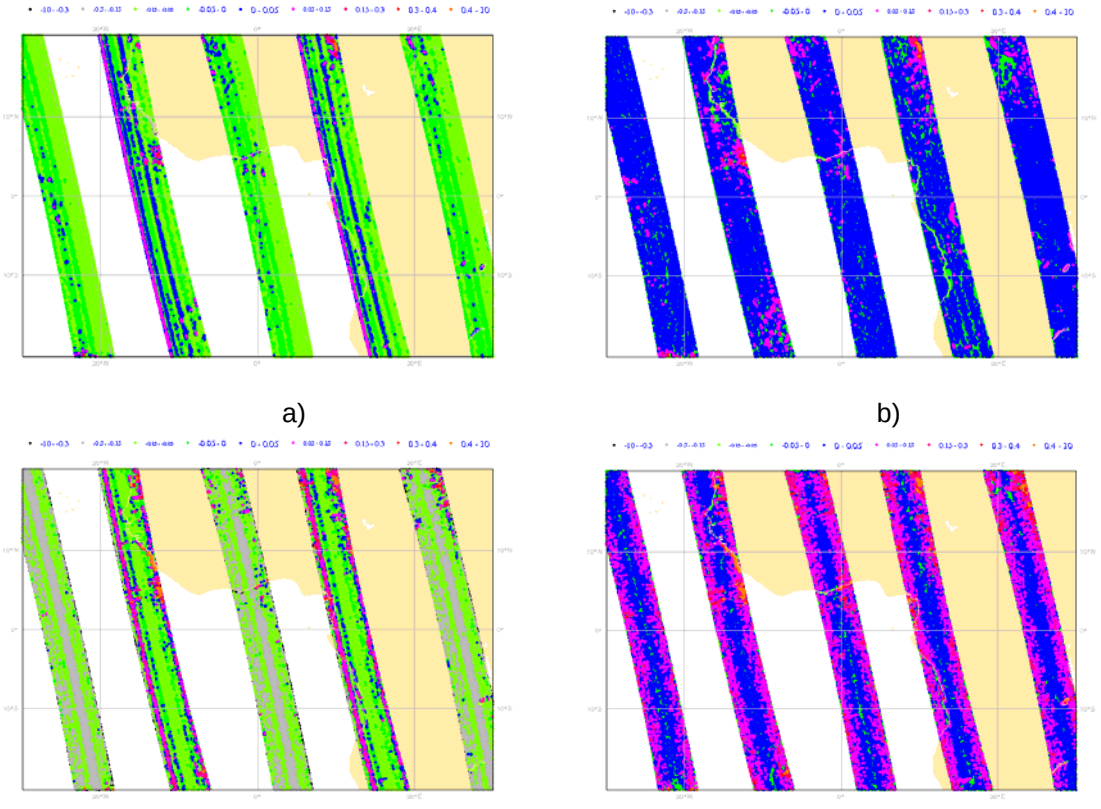

a) b)

c) d)

Figure 3 – Spatial plot (West-Africa) of the average difference in σ^0 of the PPF740-PPF730 data for the for and mid antenna . 12.5 km resolution data from ascending tracks of 2011-03-27 are used.
a) fore antenna, difference PPF740-PPF730
b) fore antenna, difference PPF740-PPF730, with corrections (Figure 2a) subtracted
c) mid antenna, difference PPF740-PPF730
d) mid antenna, difference PPF740-PPF730, with corrections (Figure 2a) subtracted

4 Total NOC correction factors

A total correction is applied to adapt the backscatter values in the level 1b stream, which consists of the NOC correction and the normalization correction as discussed in sections 2 and 3. In the following sections GMF version CMOD5.n is used in the ASCAT Wind Data Processor (AWDP) and the ocean calibration. CMOD5.n is a version of CMOD5 that is adapted for neutral winds. It is basically identical to CMOD5 with a 0.7 m/s shift in the input wind speed. The shape of the wind cone for CMOD5 and CMOD5.n is identical. The 28 fit-coefficients in the CMOD function have been recalculated for CMOD5.n by ECMWF, which lead to negligible deviations within the numerical precision of the fit procedure. The neutral wind speed GMF is the result of a triple collocation study with ECMWF winds and buoy winds [Portabella and Stoffelen 2009].

Figure 4 shows CMOD5.n and the corrected PPF740 data for the plane $z_{fore} = z_{aft}$. Figure 5 shows the same as Figure 4 but now for the projection of the wind cone and data points on the plane $z_{mid} = 0$. Figure 6 shows the intersection of the cone with the plane $z_{fore} + z_{aft} = 2z_{ref}$, for several values of z_{ref}, which correspond to (approximately) constant wind speed values. Also here the match between

measurements and GMF is good. For other WVCs similar plots have been examined (not shown). For all examined WVCs the correspondence between data and model remains good.

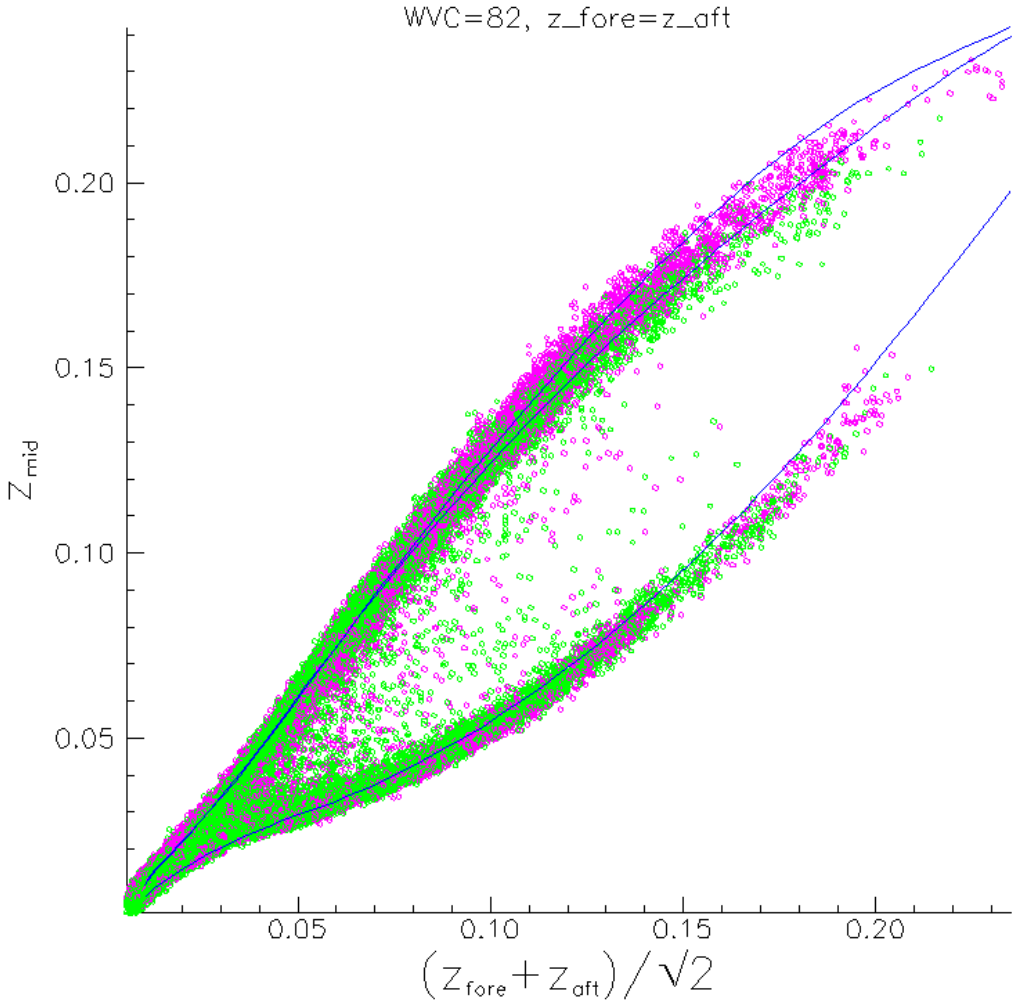

Figure 4 - Projection of the CMOD5.n wind cone (blue) and data points on the plane $z_{fore} = z_{aft.}$. Purple points belong to the upwind (outer) manifold, green points to the downwind (inner) manifold. For black points the inversion failed. Data is from level1b version PPF740, NOC corrected.

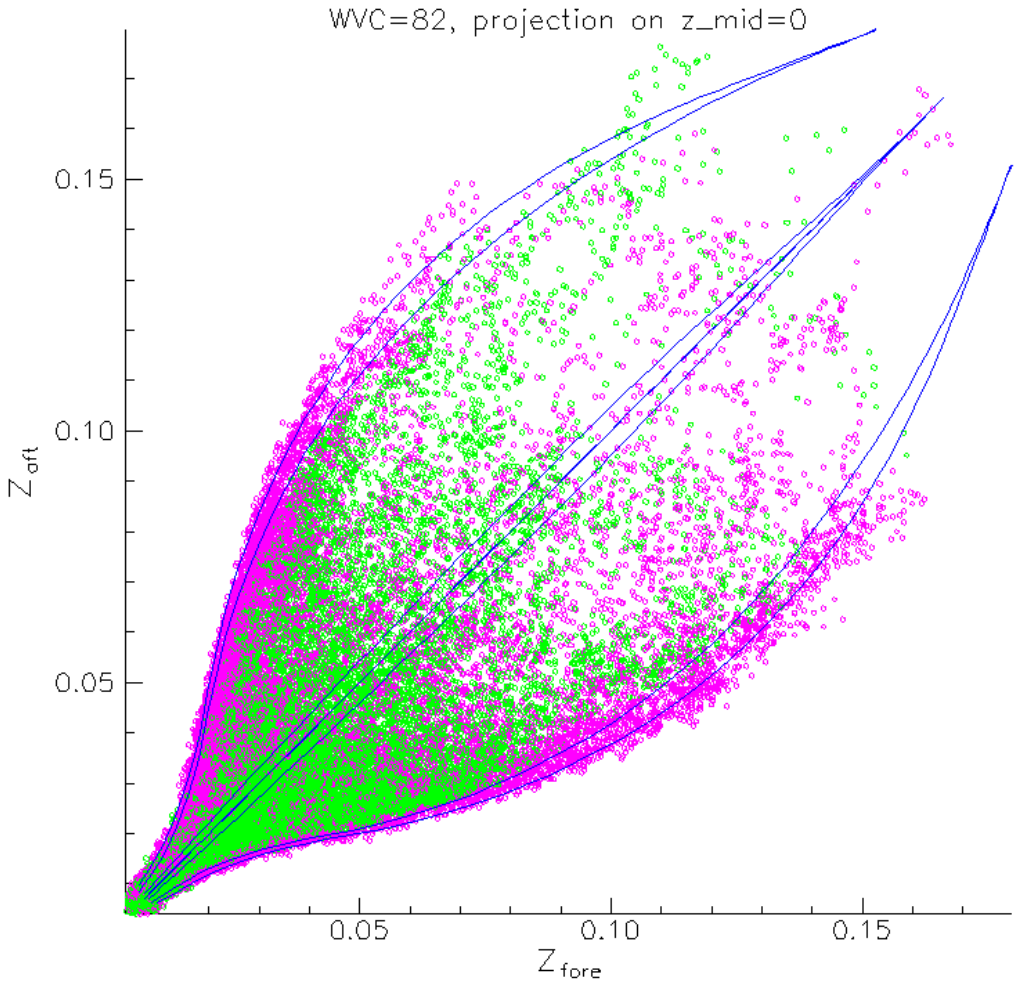

Figure 5- Projection of the CMOD5.n wind cone (blue) and data points on the plane $z_{mid} = 0$. Purple points belong to the upwind (outer) manifold, green points to the downwind (inner) manifold. For black points the inversion failed. Data is from level1b version PPF740, NOC corrected.

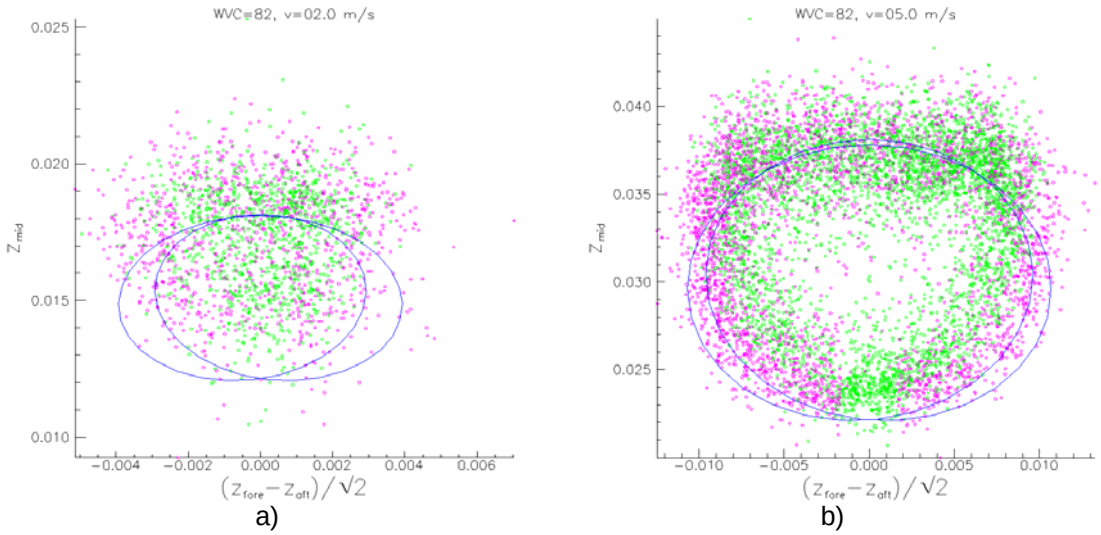

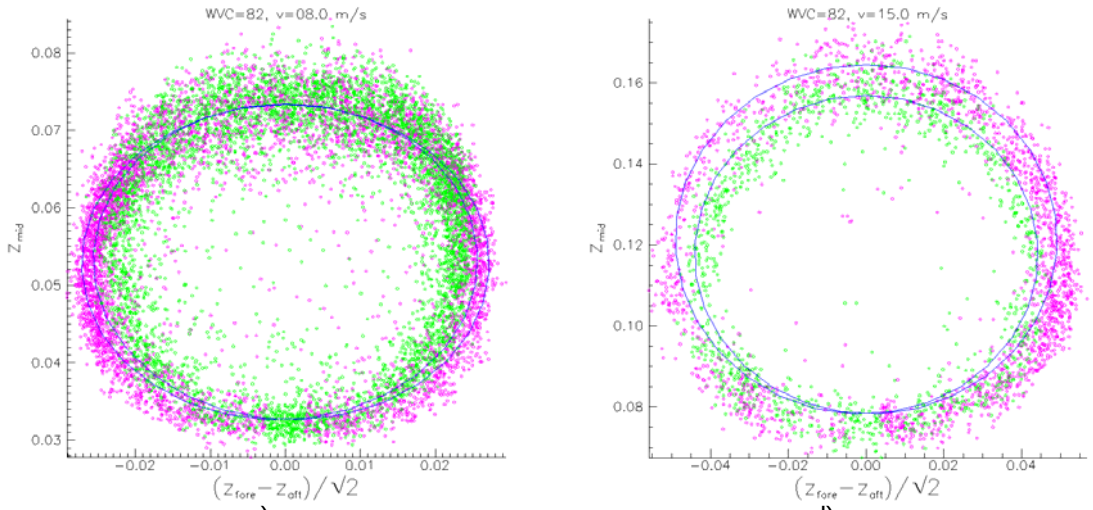

Figure 6 – Visualisation for WVC 82 of the corrected σ^0 triplets (version PPF7.4.0) and CMOD5.n (blue ellipses), for several intersections of the cone with the plane $z_{fore} + z_{aft} = 2z_{ref,}$. Purple points belong to the upwind (outer) manifold, green points to the downwind (inner) manifold. For black points the inversion failed. The plots correspond to the following wind speeds:
a) V = 2 m/s b) V = 5 m/s c) V = 8 m/s d) V = 15 m/s

The correction factors are again determined per wind vector cell (WVC) and beam. See appendix A1 for the normalisation correction factor table.

To show the effect of the correction factors in Figure 7a) and Figure 7b) the measurement space with uncorrected data is shown, analogous to Figure 4a) and Figure 6c) respectively. From this figure it is clear that correction factors are necessary and indeed do effectively remove the mismatch between data cloud and GMF.

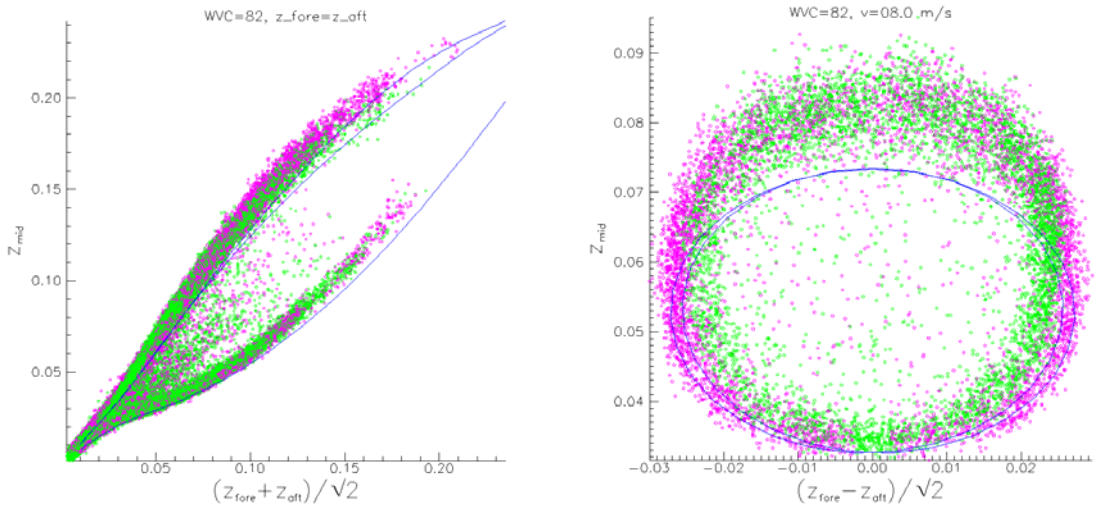

Figure 7 Visualisation in measurement space for uncorrect data from WVC 82, level1b software version PPF740. CMOD5.n is shown in blue. Purple points belong to the upwind (outer) manifold, green points to the downwind (inner) manifold. For black points the inversion failed.
a) projection of the CMOD5.n wind cone (blue) and data points on the plane zfore = zaft.
b) Intersection of the cone with the plane $z_{fore} + z_{aft} = 2z_{ref,}$, corresponding to a wind speed of 8 m/s.

Figure 8a) and b) show the total correction factor for the PPF740 and PPF730 data respectively. The correction from Figure 2a) has been added to the total correction factor for the PPF730 data in order to generate the total correction factors for the PPF740 data. The patterns look very consistent for all antennas. This is an indication that the inter-beam biases are small and that only an overall

correction, which is basically incidence angle dependent, is needed. The corrections for PPF740 look even more consistent than for PPF730, especially between the left mid beam and right mid beam. Also the wiggles in the various antenna responses have been reduced. For high incidence angles the correction is still large, i.e., around 0.8 dB. This may be caused by either a L1b calibration issue or more likely a CMOD5.n issue, since CMOD5.n has not yet been validated for such high incidence angles. We suggest ancillary sea ice, rain forest and soil geophysical comparisons to gain confidence in the backscatter calibration in the outer swath.

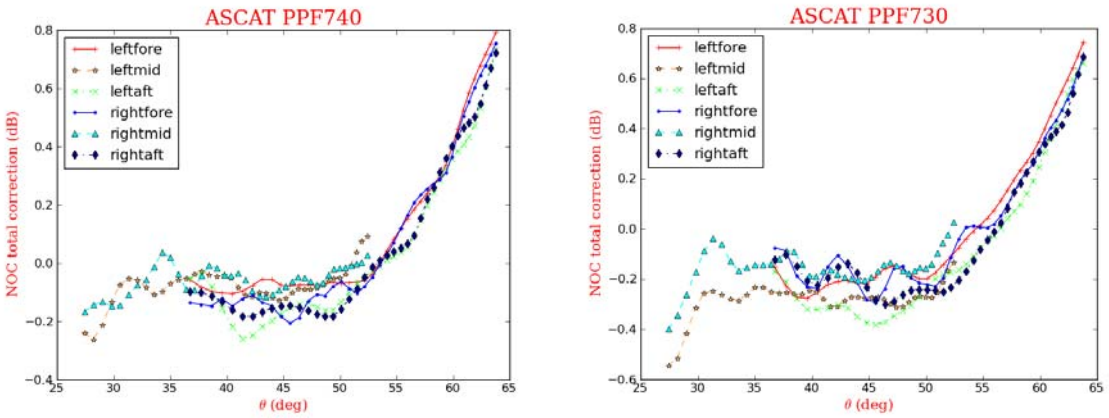

a) b)

Figure 8 – Total correction factors per antenna and incidence angle
a) PPF740 data
b) PPF730 data

The tables with total correction factors can be found in appendix A2.

5 NWP backscatter comparison

A NWP simulated backscatter comparison [VERSPEEK 2006] is performed with the parallel L1b data steams PPF740 and PPF730, both for the corrected and uncorrected case. Both L1b products are processed with AWDP using 2D-VAR ambiguity removal to provide a level 2 product with scatterometer retrieved winds and collocated NWP winds from the ECWMF model. The data is conservatively filtered to exclude land and ice. The residuals are the difference between the averaged measured σ^0 values and the averaged σ^0 values simulated from the NWP winds.

Figure 9 shows the results. Figure 9a) and Figure 9b) show the PPF740 and PPF730 residuals when using CMOD5na as GMF and no corrections. CMOD5na is a modification to CMOD5.n. A polynomial fit through the NOC residuals as a function of incidence angle θ is performed and this function $B_0^{corr}(\theta)$ is added to CMOD5.n yielding CMOD5na [VERSPEEK 2011-2]. The result is that the remaining residuals will very clearly show any interbeam bias or errors in the level 1b calibration and processing. The features shown in Figure 8 in the previous section show up even more clearly here and the same conclusions as from Figure 8 can be drawn from Figure 9a) and Figure 9b).

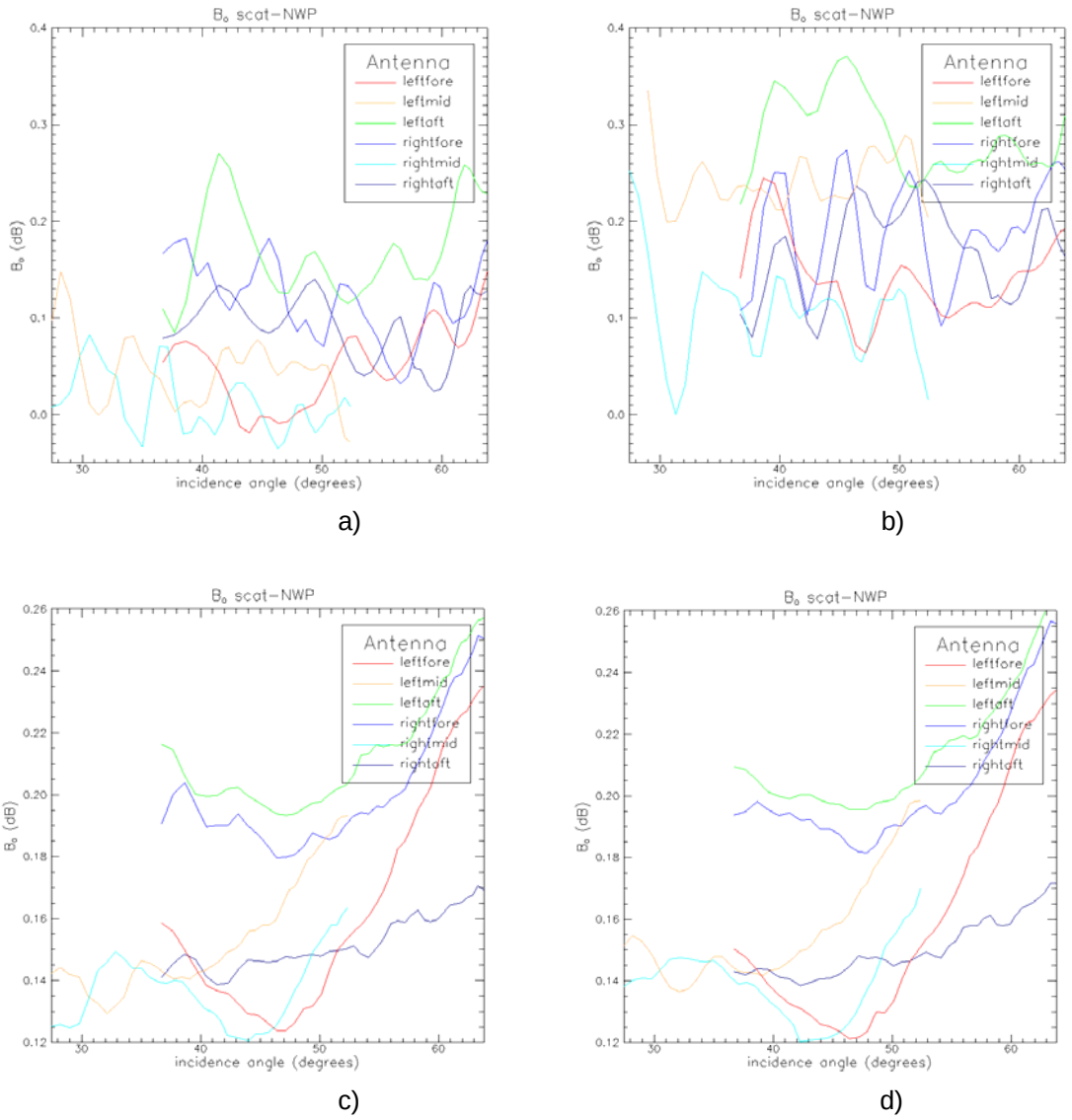

Figure 9 – Ocean calibration residuals of ASCAT backscatter values and simulated backscatter values from ECMWF 10m winds.
a) PPF740 with CMOD5na, no corrections
b) PPF730 with CMOD5na, no corrections
c) PPF740 with CMOD5n+NOC+normalisation corrections
d) PPF730 with CMOD5n+NOC+normalisation corrections

For Figure 9c) and Figure 9d) the NOC correction factors and normalisation correction factors were applied to the L1b backscatter values. The difference ranges from -0.12 dB to +0.26 dB. This is a clear improvement with respect to the uncorrected cases in Figure 8. In both cases there is a positive σ^0 bias around +0.18 dB. This corresponds to the fact that we use real 10-m ECMWF winds as input for CMOD5.n. When neutral ECWMF winds would have been used instead, the bias would be close to zero. The wiggles in the σ^0 residuals have disappeared. They have been effectively compensated for by the NOC corrections. The difference between Figure 9c) and Figure 9d) is very small. The normalisation corrections have effectively made the results alike.

6 Wind statistics

In this section some statistical plots comparing ASCAT wind and ECMWF wind are given.

First of all it is of interest to look at differences between the PPF740 corrected and PPF730 corrected wind solutions. Because the PPF740 correction incorporates the average difference between PPF740 and PPF730, both wind solutions are expected to highly correlate and show only small differences. Figure 10a) shows a scatter plot of the wind vector differences for the two data streams for one orbit. The outliers can be clearly identified and are due to selection of the “other” solution by 2DVAR ambiguity removal at low winds. They tend to clutter around the upwind and crosswind direction with respect to the mid antenna. The fraction of outliers with $|\Delta u| > 5$ m/s is in the order of 0.001. Figure 10b) shows the same plot but in a zoomed view. The points are centred around the origin with a standard deviation of 0.37 m/s in u and v direction.

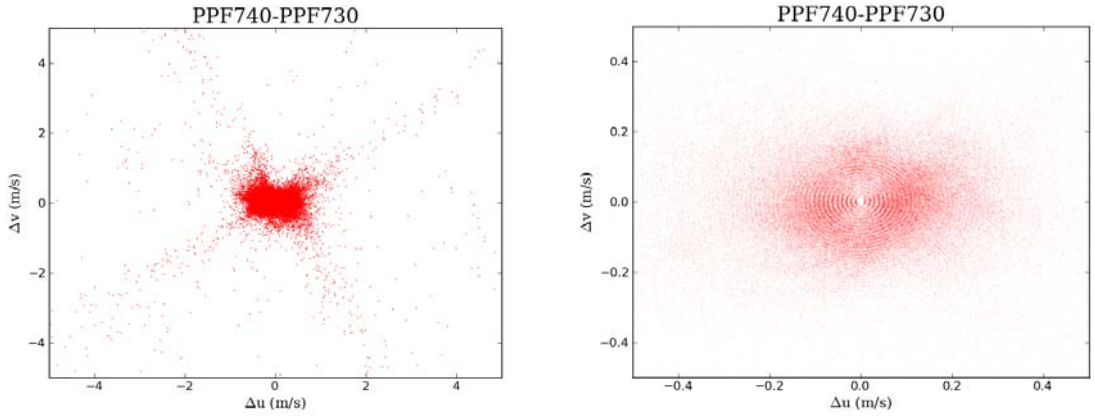

a) b)

Figure 10 – Scatter plot of the wind vector difference of PPF740 and PPF730 corrected solutions for one orbit of 12.5 km resolution data.
a) wide view b) zoomed view

Figure 11 shows the wind statistics per WVC for PPF740 and PPF730 NOC corrected data.

PPF740 data is represented in red, PPF730 in orange. The statistics for the two data sets are almost identical. This is to be expected because the PPF740-to-PPF730 correction is small and almost linear. The wind speed bias shown in Figure 11a) has an average value of ~0.17 m/s. This is due to the fact that CMOD5.n is used while we compare to real ECMWF winds rather than to neutral winds. Neutral winds have a bias of 0.2 m/s with respect to real 10 m winds. The improvement in standard deviation of wind speed and wind direction shown in Figure 11c) and Figure 11d) is merely caused by an increased rejection rate due to high Kp values that will be discussed in section 7.

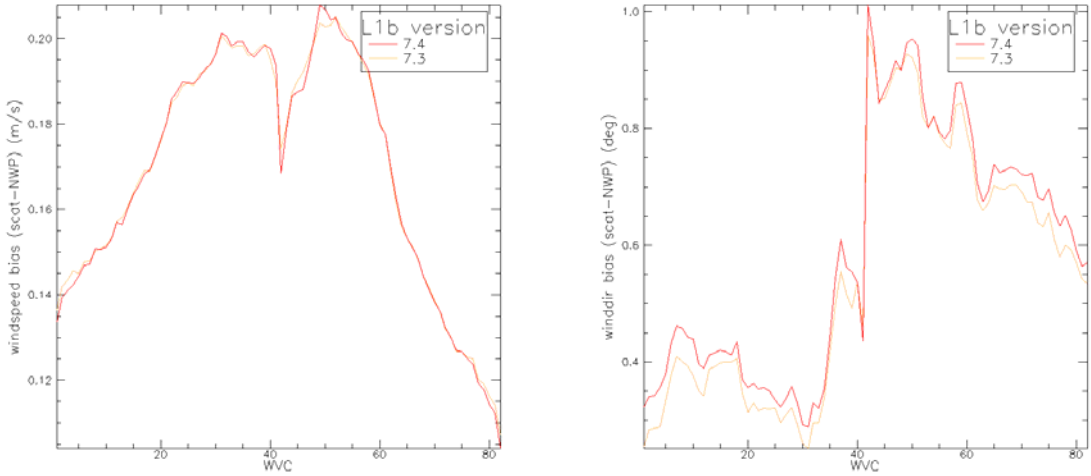

a)

b)

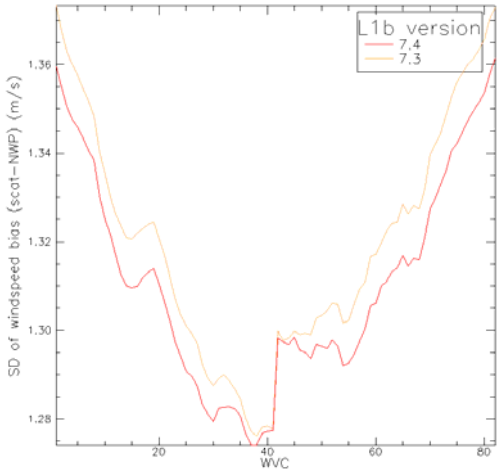

c)

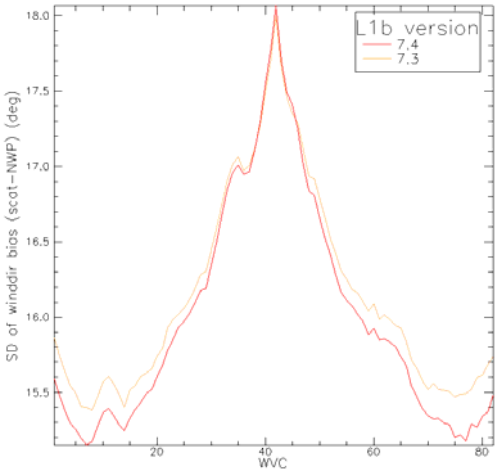

d)

Figure 11 – Wind comparison per WVC between ASCAT and ECMWF for level1b software versions PPF740 and PPF730. Backscatter data is NOC corrected. Wind direction statistics are for the 2DVAR wind solutions for ECMWF winds larger than 4 m/s.
a) wind speed bias b) wind direction bias
c) wind speed SD d) wind direction SD.

Figure 12 shows the wind scatter plots for PPF740 NOC corrected data. PPF730 wind scatter plots and statistics are very similar in terms of wind performance, as may be expected from Figure 10.

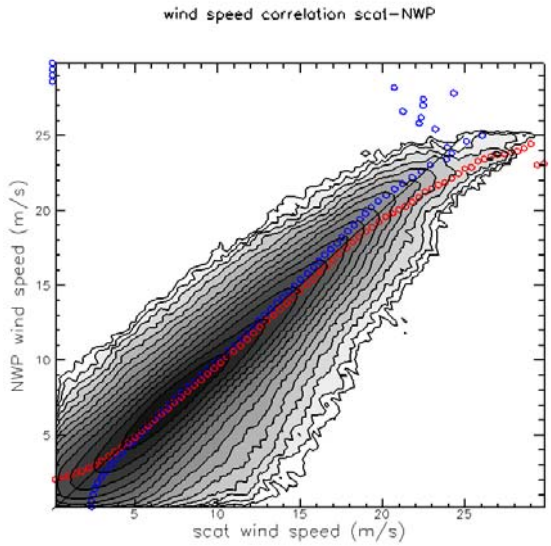

N= 23171876
mx=7.86 my= 7.69
cor_xy=0.93

a)

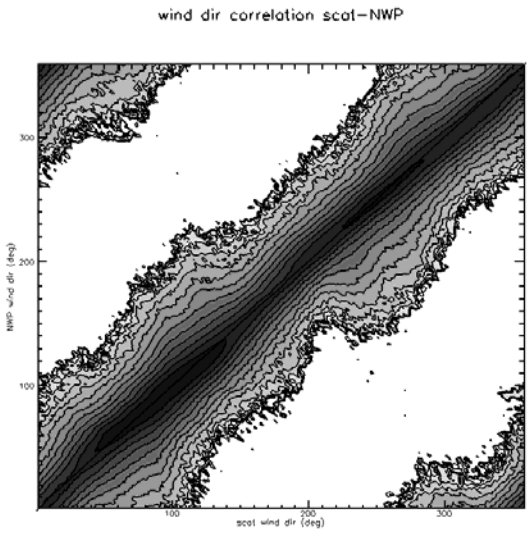

N=19731133
mx=165.75 my=167.96

b)

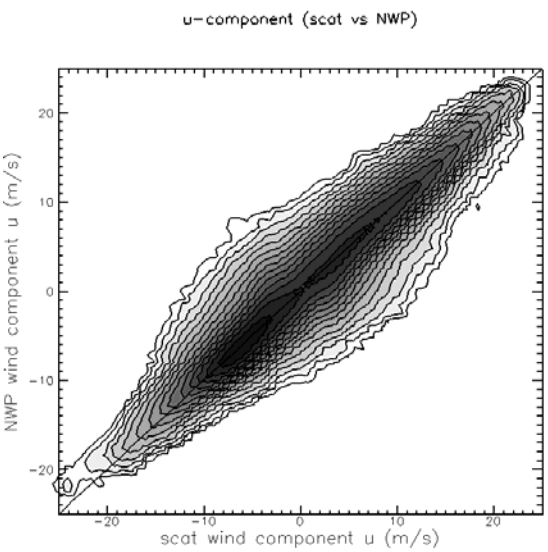

N= 23171876
mx= -0.54 my= -0.38
cor_xy= 0.97

c)

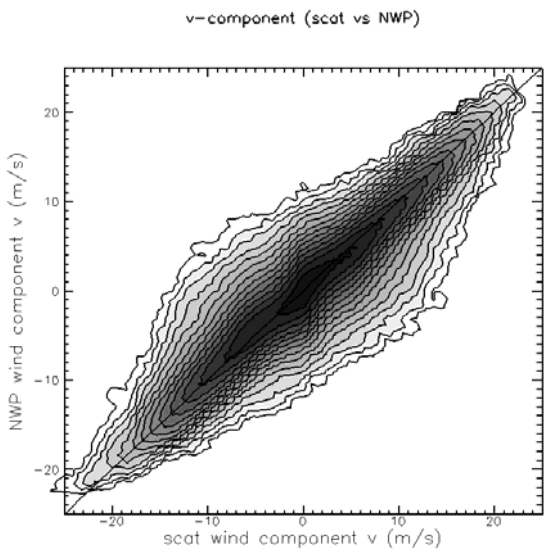

N= 23171876
mx=0.06 my=0.09
cor_xy= 0.95

d)

Figure 12 – Two-dimensional histogram of the 2D-VAR KNMI-retrieved wind solution versus ECMWF wind for all WVCs. The PPF740 data with NOC correction is used. N is the number of data; mx and my are the mean values along the x and y axis, respectively; and cor_xy is the correlation coefficient for the xy distribution. The contour lines are in logarithmic scale: each level up is a factor of 2. Lowest level=10, there are 15 levels in total.
a) wind speed (bins of 0.4 m/s). The red dots show <Vnwp> for each Vscat bin, the blue dots show <Vscat> for each Vnwp bin.
b) wind direction (bins of 2.5°) for ECMWF winds larger than 4 m/s.
c) wind component u (bins of 0.4 m/s).
d) wind component v (bins of 0.4 m/s).

7 MLE statistics and QC

Figure 13 shows the normalised distance to cone or Maximum Likelihood Estimator (MLE) [PORTABELLA and STOFFELEN 2006] as a function of WVC for PPF740 NOC corrected data. The data range is divided into 15 levels equally spaced on a logarithmic scale, each successive level is a factor of two higher than the previous level. For low MLE values there is no dependency on WVC number. For higher MLE values a dependency on WVC number can be seen that is symmetric for the left and right swath, so in fact the dependency is on incidence angle. The plot for PPF730 NOC corrected data is very similar.

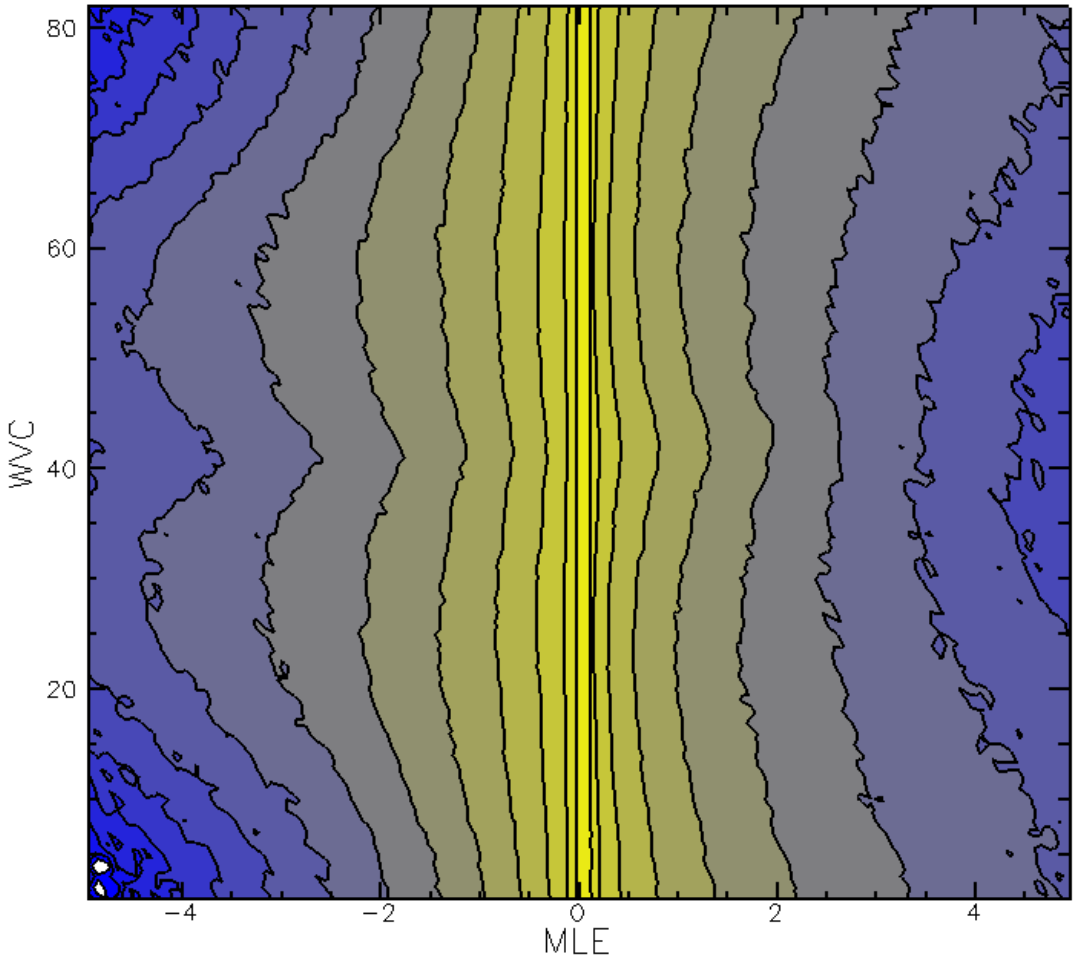

Figure 13 - MLE distribution per WVC shown for PPF740 NOC corrected data. The data range is divided into 15 levels equally spaced on a logarithmic scale, each successive level is a factor of 2 higher than the previous level.

Figure 14 shows the MLE as a function of the scatterometer wind speed for PPF740 NOC corrected dataa. For high wind speed values the cone cross section is large compared to the spread of the triplets around the cone surface. A symmetrical pattern around the origin is expected here as an equal amount of triplets are on the inner and outer side of the cone surface (see Figure 6). For low wind speed values, i.e. smaller than ~4 m/s, the cone radius is small and the spread of triplets is relatively large. More triplets are expected to lie outside the cone and thus have a negative MLE.

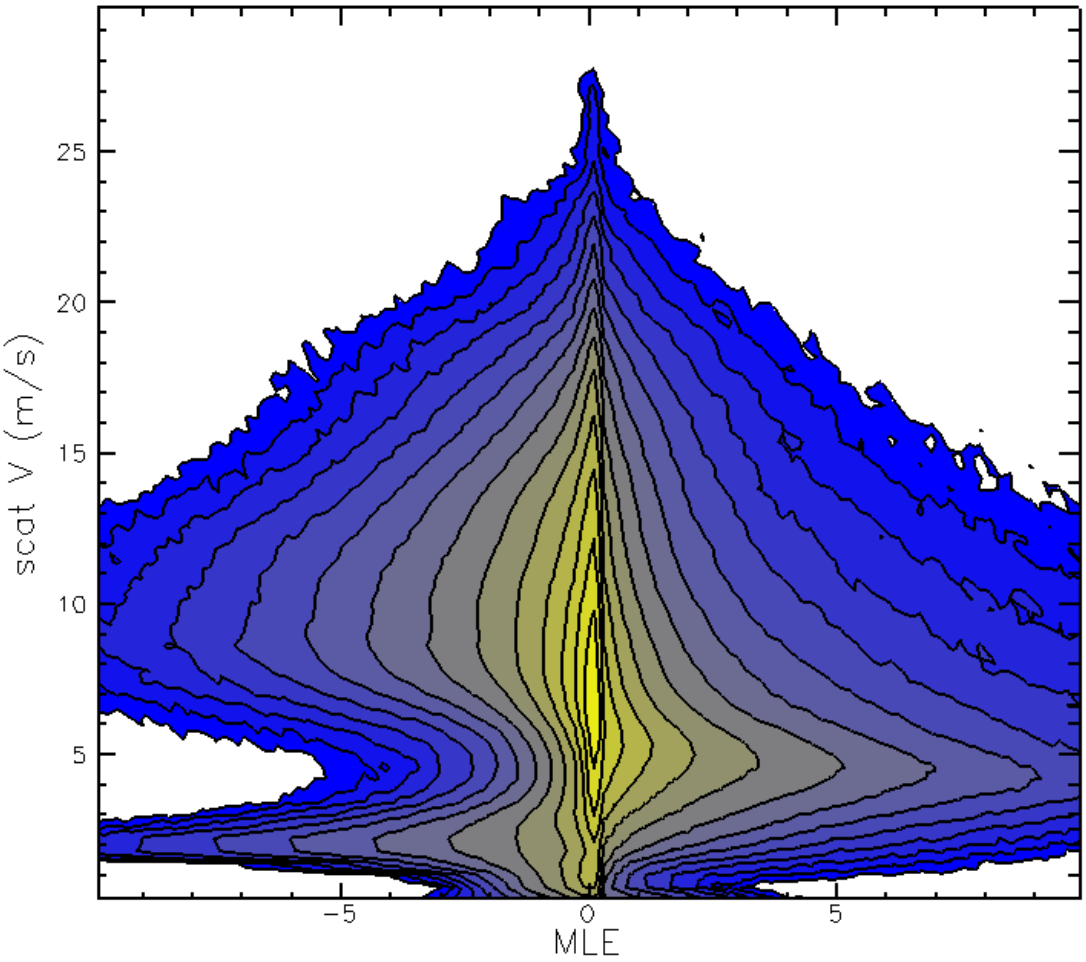

Figure 14 – Cone distance distribution versus measured wind speed for PPF740 data.

Note that around 5 m/s most corrected triplets lie within the cone. This corresponds to earlier assessments that the CMOD5.n cone is too wide for these winds [Portabella and Stoffelen, 2006]. After the ASCAT Cal/Val, we anticipate to use the MLE to correct CMOD5.n.

The MLEs in the ASCAT BUFR product have been normalised. In order to compute a normalisation table, ASCAT 25-km data from 20 September 2008 to 19 October 2008 (both inclusive) have been reprocessed. In the wind inversion, the CMOD5.n GMF for neutral winds was used [VERHOEF et al 2008] and the appropriate backscatter correction (PPF740) was applied. All WVCs with latitude above 55 degrees North or below 55 degrees South were skipped to exclude any ice contamination. Only those wind solutions closest to the ECMWF forecast winds and with wind speeds above 4 m/s have been used. No quality control regarding maximum acceptable MLE values was applied. Using these data, for each WVC number (1 to 42), the mean absolute cone distance was calculated: <MLE1>.

The reprocessing was repeated, but in this second step the MLEs were normalised using the <MLE1> table obtained in the first step. Moreover, WVCs with an absolute normalised MLE above

18.45 were skipped, yielding a rejection rate of approximately 0.4 to 0.5%. For the accepted data, the mean absolute cone distance vs. WVC number was calculated again: <MLE2>. The final MLE normalisation table was computed as the product of the mean values from step 1 and 2 WVC-by-WVC: <MLE> = <MLE1> <MLE2>. Also, a quality control threshold table QC (again as a function of WVC number) was computed as QC = 18.45 / <MLE2>. WVCs with a normalised absolute MLE value above the QC table value are rejected in the wind processing software. In this way, we keep the rejection rate at 0.4 to 0.5%.

The justification for the MLE threshold of 18.45 is that we looked for a value that produced a rejection rate of about 0.4%, which was the initial rejection rate of the AWDP ASCAT quality control before any development or tuning. The reason for this is that we discovered that users were very satisfied with such a low rejection rate, as compared to the rejection rate of 1-2% that was obtained in the ERS processing in the past. Actually we see that there is no sharp cut in the MLE (with respect to the quality of the data) but rather a smooth degradation of the quality of the winds as the MLE increases.

Using the MLE normalisation table that we thus obtained for wind speeds above 4 m/s, i.e. <MLE>, we also looked at the MLE characteristics as a function of wind speed and WVC number for low wind speeds. It appears that the MLEs strongly increase below 2 m/s. This also leads to a strong increase of the rejection rate at low wind speeds, which is generally undesirable: for wind speeds below 2 m/s, the wind speed and wind component deviations from the true wind are almost always small and well within the product specification. Hence we decided to apply an extra normalisation to the MLEs below 2 m/s. A wind speed dependent parabolic function (not shown) was fitted to the mean MLEs below 2 m/s and this function is used as an extra (WVC independent) correction value for the MLEs. Details on the MLE normalisation and QC threshold setting for NOC corrected data can be found in [VERSPEEK 2011].

Figure 15 shows the average absolute MLE after applying the <MLE> normalisation and using the QC threshold. The mean MLE is not exactly equal to 1 since in this plot also low winds (for which an ad-hoc normalisation using the parabolic function is performed) are taken into account. The mean MLE of the selected solutions is around 0.8 and reasonably constant over the swath.

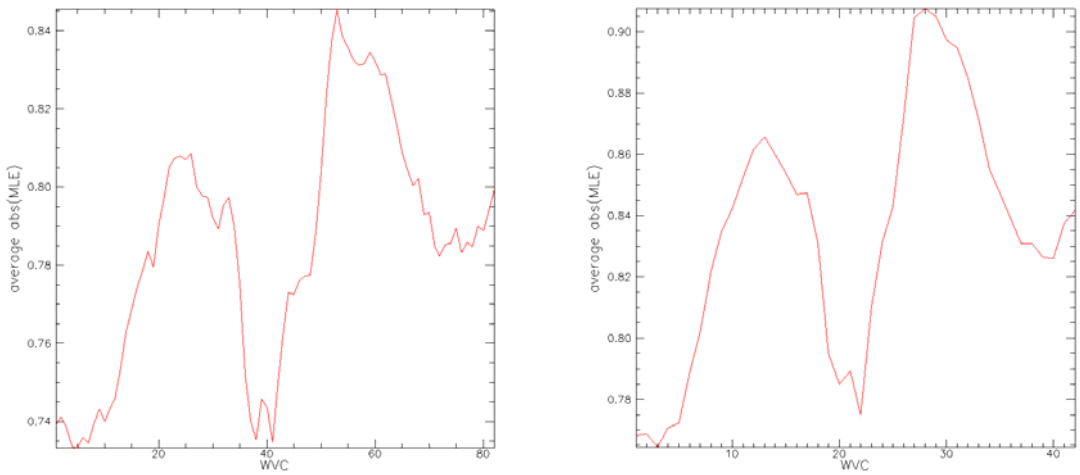

a) b)

Figure 15 – ASCAT average MLE as a function of WVC number. Results are shown for all wind speeds, including those below 4 m/s, Level 1b version 7.4 data is used with NOC corrections applied.
a) 12.5 km resolution
b) 25 km resolution

Figure 16 shows the instrument noise Kp for level 1B software versions PPF740 and PPF730 as a function of WVC number per antenna. The jump in Kp at WVC 20 for the fore and aft antennas is caused by a transition from 6 to 8 looks in the full-resolution product.. A new algorithm has been

implemented for the calculation of the Kp value out of the full-resolution product. The new algorithm takes the weight-factors into account, as the backscatter is a weighted average over the full-resolution radar return signals [ANDERSON 2011]. The new algorithm generally leads to a higher value for Kp.

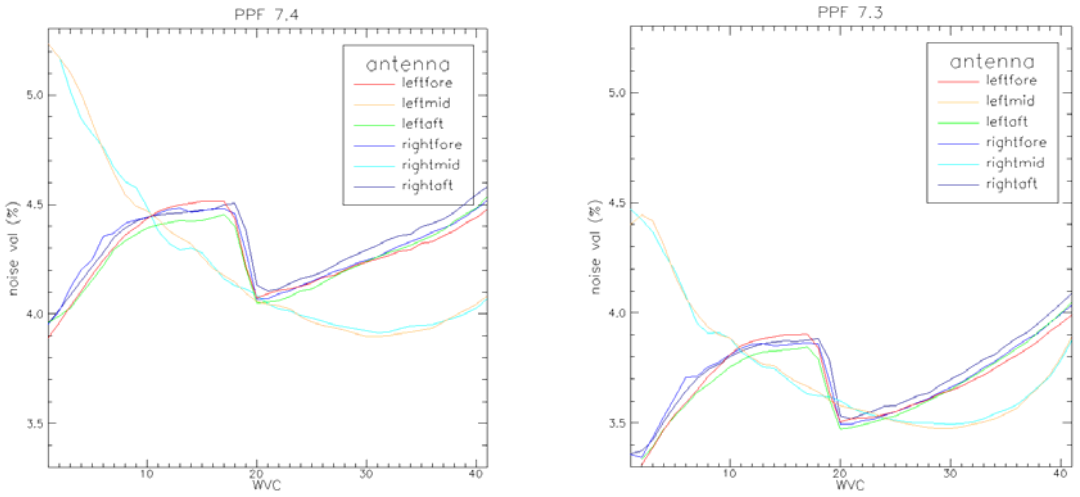

a) b)

Figure 16 – Averaged instrument noise Kp as a function of WVC number per antenna for a) level 1B software version PPF740 and b) version PPF730.

Figure 17 shows some level 2 quality flag occurrences as a function of WVC number. Figure 17a) and b) show the 12.5 km resolution of version PPF740 and PPF730 respectively, and Figure 17c) and d) show the same for the 25 km resolution. An overall increase in kp quality flag occurrence can be noticed for both the 12.5 km and 25 km resolution. This is caused by the new Kp algorithm implemented at EUMETSAT as described before.

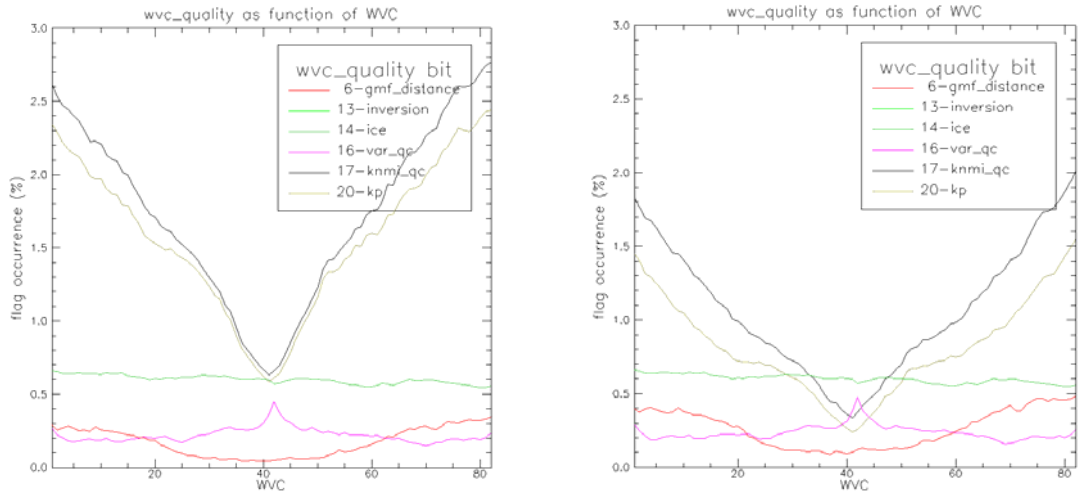

a) b)

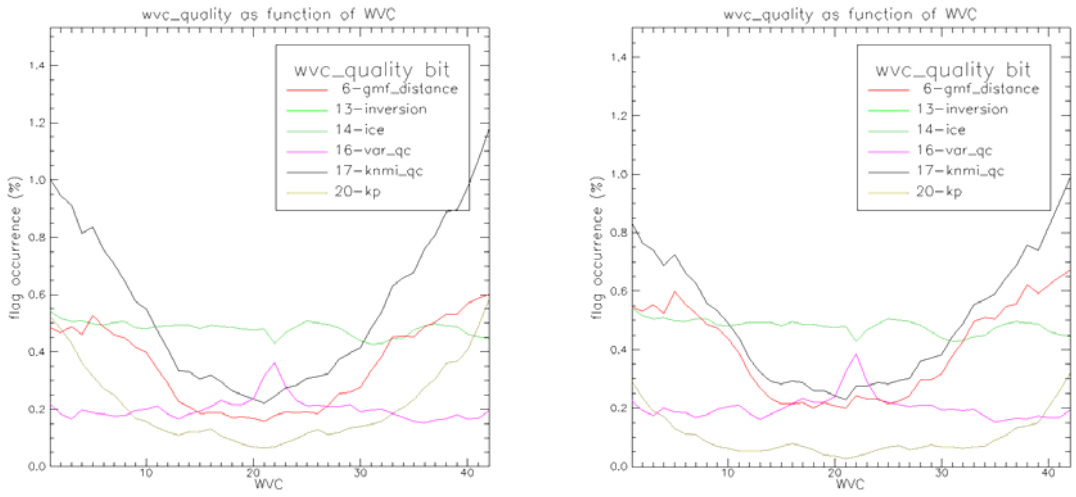

c) d)

Figure 17 – ASCAT quality flags occurrence as a function of WVC number. Results are shown for all wind speeds, including those below 4 m/s, Level 1b version PPF740 and PPF730 data is used with NOC corrections applied.
a) 12.5 km resolution version PPF740
b) 12.5 km resolution version PPF730
c) 25 km resolution version PPF740
d) 25 km resolution version PPF730

In the 12.5 km resolution mode clearly the Kp quality flag is dominating as contributor to the knmi_qc flag. Its influence can be reduced by relaxing the Kp-threshold setting for the 12.5 km resolution in the level 2 processing to obtain the same profile as for the 25 km resolution, i.e., a relaxation by a factor of two. This would slightly decrease the swath wind accuracy by about 0.02 m/s and a 10^{th} of a degree in wind direction (cf. figure 11), but with a considerable reduction in QC rejections. The distance-to-cone check and the Kp check work in a similar manner, but the former is supposed to be the main mechanism for detecting backscatter anomalies for wind retrieval.

The rejection rate increases when we go from the inner part to the outer part of the swath. This can be explained as follows. The cone opens up with incidence angle. Therefore, larger MLE values inside the cone are more frequent in the outer swath (less aliasing effect). Also noise is somewhat larger at higher incidence angles. These effects broaden the MLE distribution at high incidence angles and therefore increases the QC rejection rate.

Routine monitoring statistics are accessible through the OSI SAF ASCAT product viewer web site: http://www.knmi.nl/scatterometer/ascat_osi_25_prod/ascat_app.cgi by selecting “Monitoring information”.

8 Conclusions

Based on the OSI SAF cone visualisation tools at KNMI and the NOC method calibration of the ASCAT scatterometer is attempted. CMOD5n was carefully derived for the ERS scatterometer and thus our calibration should result in the compatibility of the ERS and ASCAT scatterometer products. Indeed, the scatterometer wind product of ASCAT is shown to have similar characteristics to the ERS scatterometer wind product and meets the wind product requirements.

ECMWF short range forecast winds are used here as reference. With the implementation of new ECMWF model cycles the ECMWF winds may become more or less biased. ECMWF verification statistics indicate that the low bias of ECMWF winds at the beginning of this century (e.g. [HERSBACH 2007]) have compensated by more recent ECMWF model cycles [HERSBACH,

personal communication). Moreover, the random wind component errors in ECMWF and ERS scatterometer winds and their respective spatial representation are generally different. These differences may result in absolute overall biases of a few 10^{th} of a m/s; which results in a few 10^{th} of dB uncertainties in backscatter as well, however, rather uniformly spread over the WVCs [STOFFELEN 1999].

The ASCAT PPF740 L1b backscatter data, is compared to the currently used PPF730 L1b backscatter data. For the corrected case, consistency between the two sets is found, and the new "PPF740" set shows smaller interbeam differences, and the former offset in the left mid beam antenna response has disappeared, and former "wiggles" in antenna responses have been reduced, suggesting improved L1b calibration. In the outer swath consistent large departures remain for the uncorrected case. The level 2 monitoring statistics, like average MLE, average wind speed bias with respect to the NWP wind speed, SD of the wind speed and wind direction show almost identical pictures for the PPF740 and PPF730 corrected data.

An overall increase in Kp quality flag occurrence can be noticed for both the 12.5 km and 25 km resolution. This is caused by the new Kp algorithm implemented at EUMETSAT. In the 12.5 km resolution mode clearly the Kp quality flag is dominating as contributor to the knmi_qc flag. It is recommended to relax the Kp-threshold setting for the 12.5 km resolution product in AWDP.

When using the correction table, the level 2 wind product is of high quality. The aim is to get also a high-quality product without using a correction table. Of course, this could be easily achieved by incorporating the correction table in the CMOD fit-parameters.

The current corrections may be split in a GMF dependent part, which lead to the development of CMOD5na, and a remaining antenna-dependent part, named NOCa. Initial results for CMOD5na+NOCa are promising and show very little difference in wind quality compared to the present CMOD5n+NOC combination. The current NOCa corrections from the ocean calibration are relevant and uncorrected (CMOD5na) wind retrievals are not acceptable as a level 2 wind product. This issue should be resolved by checking against other ancillary geophysical data like from sea ice or rain forest surfaces. This could be done by making the NOCa corrections available for these other products. This will help in resolving any remaining errors in, and assessing the validity of, the CMOD5na GMF and L1b calibration, especially for the high incidence angles.

Appendix A1 – Normalisation correction table for PPF740 to PPF730

The PPF740-PPF7300 normalisation correction factors (dB) as a function of WVC and beam for level 1b version PPF7.4.0 This table is copied from awdp_tables.F90. All other normalisation and NOC tables can also be found in awdp_tables.F90:

```
real, public, parameter, dimension(3, 42) :: PPF740_PPF730 = &
& reshape((/ &
!          fore             mid             aft          WVC
&  0.0491216779,  0.2339349240,  0.0749431625,& !        1
&  0.0741123781,  0.2472979873,  0.0204478130,& !        2
&  0.0833247676,  0.2368329167,  0.0106915683,& !        3
&  0.0715792254,  0.2223740965,  0.0502690859,& !        4
&  0.0479178727,  0.2201206237,  0.1064242497,& !        5
&  0.0351664647,  0.2156254649,  0.1358111799,& !        6
&  0.0470025763,  0.1915938407,  0.1223498136,& !        7
&  0.0674543679,  0.1626400501,  0.0949696824,& !        8
&  0.0707231164,  0.1616159827,  0.0915157795,& !        9
&  0.0529696979,  0.1820696592,  0.1137874052,& !       10
&  0.0487175994,  0.1965580732,  0.1266795397,& !       11
&  0.0809939280,  0.2020357251,  0.1139135212,& !       12
&  0.1147888601,  0.2120908946,  0.1103064492,& !       13
&  0.1066388264,  0.2161434591,  0.1479501575,& !       14
&  0.0908546671,  0.1937965602,  0.2011490315,& !       15
&  0.1150840223,  0.1710261703,  0.2057146579,& !       16
&  0.1420959383,  0.1809860617,  0.1422612816,& !       17
&  0.1385128945,  0.1920581907,  0.0842834041,& !       18
&  0.1487949193,  0.1826629937,  0.1156541109,& !       19
&  0.1462981850,  0.2195623368,  0.1553411931,& !       20
&  0.0573837608,  0.3059579730,  0.1064248234,& !       21
&  0.0411227606,  0.2083124071,  0.0699237138,& !       22
&  0.0193028264,  0.1107679605,  0.0353857800,& !       23
&  0.0582766719, -0.0160341561,  0.0373659655,& !       24
&  0.0301724058,  0.0001192564,  0.0006311740,& !       25
&  0.0507036075,  0.1158812344,  0.0274859294,& !       26
&  0.0708795488,  0.1377207041,  0.1046826020,& !       27
&  0.0537209697,  0.0729686394,  0.1148708314,& !       28
&  0.0863103643,  0.0578709058,  0.0802730322,& !       29
&  0.1282445788,  0.1080681607,  0.0932910964,& !       30
&  0.0881947353,  0.1342471987,  0.1482791901,& !       31
&  0.0203652512,  0.1108020395,  0.1756841838,& !       32
&  0.0306689143,  0.0887288228,  0.1484314352,& !       33
&  0.1006661952,  0.0966882631,  0.1031101272,& !       34
&  0.1375977248,  0.1068495959,  0.0766030997,& !       35
&  0.1100371554,  0.0975567773,  0.0751849040,& !       36
&  0.0697703511,  0.0911428183,  0.0861512423,& !       37
&  0.0679622293,  0.1094608903,  0.0946975350,& !       38
&  0.0998593122,  0.1312490404,  0.0959790275,& !       39
&  0.1232077777,  0.1148580536,  0.0881734192,& !       40
&  0.1100593358,  0.0629693195,  0.0694682971,& !       41
&  0.0697369128,  0.0168079957,  0.0376824737 & !       42
&  /), (/3, 42/)) ! (iBeam, iNode)
```

Appendix A2 – Total NOC correction table for PPF740

The total NOC correction factors (dB) as a function of WVC and beam for level 1b version PPF7.4.0 This table is copied from awdp_prepost.F90. All other total NOC correction tables can also be found in awdp_prepost.F90:

total correction factors in dB for PPF740

```
#                    fore                        mid                         aft
tot_cf(1, 1) =  0.8018716779 ; tot_cf(2, 1) =  0.0859305073 ; tot_cf(3, 1) =  0.7325258708
tot_cf(1, 2) =  0.7181340448 ; tot_cf(2, 2) =  0.0366328206 ; tot_cf(3, 2) =  0.6042055213
tot_cf(1, 3) =  0.6295362676 ; tot_cf(2, 3) = -0.0244297083 ; tot_cf(3, 3) =  0.4839094016
tot_cf(1, 4) =  0.5176335171 ; tot_cf(2, 4) = -0.0571292368 ; tot_cf(3, 4) =  0.4064279192
tot_cf(1, 5) =  0.3947779144 ; tot_cf(2, 5) = -0.0776668346 ; tot_cf(3, 5) =  0.3473067080
tot_cf(1, 6) =  0.2975472147 ; tot_cf(2, 6) = -0.0927377434 ; tot_cf(3, 6) =  0.2745190132
tot_cf(1, 7) =  0.2325232430 ; tot_cf(2, 7) = -0.1039539926 ; tot_cf(3, 7) =  0.1845415636
tot_cf(1, 8) =  0.1741605346 ; tot_cf(2, 8) = -0.1228798249 ; tot_cf(3, 8) =  0.0940875574
tot_cf(1, 9) =  0.1079525331 ; tot_cf(2, 9) = -0.1256100173 ; tot_cf(3, 9) =  0.0319477378
tot_cf(1,10) =  0.0304863229 ; tot_cf(2,10) = -0.1214661325 ; tot_cf(3,10) = -0.0035836365
tot_cf(1,11) = -0.0386470673 ; tot_cf(2,11) = -0.1112376768 ; tot_cf(3,11) = -0.0406098353
tot_cf(1,12) = -0.0712857387 ; tot_cf(2,12) = -0.0784461916 ; tot_cf(3,12) = -0.0859960621
tot_cf(1,13) = -0.0804471816 ; tot_cf(2,13) = -0.0607186887 ; tot_cf(3,13) = -0.1411249258
tot_cf(1,14) = -0.0845171736 ; tot_cf(2,14) = -0.0590661659 ; tot_cf(3,14) = -0.1660108008
tot_cf(1,15) = -0.0895250829 ; tot_cf(2,15) = -0.0775878148 ; tot_cf(3,15) = -0.1630972185
tot_cf(1,16) = -0.0924973527 ; tot_cf(2,16) = -0.1103278297 ; tot_cf(3,16) = -0.1812702588
tot_cf(1,17) = -0.0905734784 ; tot_cf(2,17) = -0.1239095216 ; tot_cf(3,17) = -0.2255981351
tot_cf(1,18) = -0.1105183555 ; tot_cf(2,18) = -0.1095731843 ; tot_cf(3,18) = -0.2642443459
tot_cf(1,19) = -0.1373356640 ; tot_cf(2,19) = -0.1540148396 ; tot_cf(3,19) = -0.2325020558
tot_cf(1,20) = -0.1401801900 ; tot_cf(2,20) = -0.2636431632 ; tot_cf(3,20) = -0.1516758069
tot_cf(1,21) = -0.1275123642 ; tot_cf(2,21) = -0.2425632770 ; tot_cf(3,21) = -0.1698903433
tot_cf(1,22) = -0.1872681977 ; tot_cf(2,22) = -0.2806181762 ; tot_cf(3,22) = -0.1606082445
tot_cf(1,23) = -0.1910043819 ; tot_cf(2,23) = -0.2102294145 ; tot_cf(3,23) = -0.1692098033
tot_cf(1,24) = -0.1746359531 ; tot_cf(2,24) = -0.1800489478 ; tot_cf(3,24) = -0.1933144928
tot_cf(1,25) = -0.1601948025 ; tot_cf(2,25) = -0.1229574936 ; tot_cf(3,25) = -0.2030069510
tot_cf(1,26) = -0.1782998925 ; tot_cf(2,26) = -0.0554334323 ; tot_cf(3,26) = -0.1840278623
tot_cf(1,27) = -0.1985283679 ; tot_cf(2,27) = -0.0384197959 ; tot_cf(3,27) = -0.1712463980
tot_cf(1,28) = -0.1646166970 ; tot_cf(2,28) = -0.0821969023 ; tot_cf(3,28) = -0.1783563353
tot_cf(1,29) = -0.1176769274 ; tot_cf(2,29) = -0.0734982609 ; tot_cf(3,29) = -0.1873039678
tot_cf(1,30) = -0.0973163795 ; tot_cf(2,30) = -0.0479640060 ; tot_cf(3,30) = -0.1628154036
tot_cf(1,31) = -0.0929345980 ; tot_cf(2,31) = -0.0573003013 ; tot_cf(3,31) = -0.1006528516
tot_cf(1,32) = -0.0539669988 ; tot_cf(2,32) = -0.0816801688 ; tot_cf(3,32) = -0.0333028579
tot_cf(1,33) =  0.0202331226 ; tot_cf(2,33) = -0.1145149272 ; tot_cf(3,33) =  0.0131419352
tot_cf(1,34) =  0.1067630285 ; tot_cf(2,34) = -0.1153900286 ; tot_cf(3,34) =  0.0473941689
tot_cf(1,35) =  0.1892595998 ; tot_cf(2,35) = -0.0893081124 ; tot_cf(3,35) =  0.1034842664
tot_cf(1,36) =  0.2455317387 ; tot_cf(2,36) = -0.0661231394 ; tot_cf(3,36) =  0.2008387373
tot_cf(1,37) =  0.2896155178 ; tot_cf(2,37) = -0.0667160150 ; tot_cf(3,37) =  0.3045409506
tot_cf(1,38) =  0.3726118543 ; tot_cf(2,38) = -0.0597727764 ; tot_cf(3,38) =  0.3931667017
tot_cf(1,39) =  0.4938259789 ; tot_cf(2,39) = -0.0300710429 ; tot_cf(3,39) =  0.4581851942
tot_cf(1,40) =  0.5983423610 ; tot_cf(2,40) = -0.0109126964 ; tot_cf(3,40) =  0.5174092525
tot_cf(1,41) =  0.6820125025 ; tot_cf(2,41) =  0.0061174028 ; tot_cf(3,41) =  0.6133651721
tot_cf(1,42) =  0.7612789545 ; tot_cf(2,42) =  0.0473044124 ; tot_cf(3,42) =  0.7235131404
```

Acronyms and abbreviations

Name	Description
AMI	Active Microwave Instrument
ASCAT	Advanced scatterometer
AWDP	Ascat Wind Data Processor
BUFR	Binary Universal Form for Representation (of meteorological data)
CMOD	C-band geophysical model function used for ERS and ASCAT
ECMWF	European Centre for Medium-Range Weather Forecasts
ERA40	ECMWF 40 year reanalysis
ERS	European Remote sensing Satellite
ESA	European Space Agency
ESDP	ERS Scatterometer Data Processor
EUMETSAT	European Organization for the Exploitation of Meteorological Satellites
GMF	geophysical model function
KNMI	Koninklijk Nederlands Meteorologisch Instituut (Royal Netherlands Meteorological Institute)
METOP	Meteorological Operational satellite
MLE	maximum likelihood estimator (used for distance to cone)
NWP	numerical weather prediction
OSI	Ocean and Sea Ice
QC	Quality Control (inversion and ambiguity removal)
SAF	Satellite Application Facility
SD	standard deviation
WVC	wind vector cell, also known as node or cell

Table 1 - List of acronyms and abbreviations

References

[ANDERSON 2011] Anderson, Craig, Technical Note on Kp calculation, EUMETSAT, Darmstadt Germany, 2011

[BELMONTE 2012] Belmonte, M., J. Verspeek, A. Verhoef and A. Stoffelen, Bayesian sea ice detection with the Advanced Scatterometer, IEEE Transactions on Geoscience and Remote Sensing, 2012, 50, 7, 2649-2657, doi:10.1109/TGRS.2011.2182356.

[FIGA 2004] Figa-Saldaña, Julia, "ASCAT calibration and validation plan", *EUMETSAT*, EPS programme, Darmstardt Germany, 2004

[FIGA et al 2002] Figa-Saldaña, J., J.J.W. Wilson, E. Attema, R. Gelsthorpe, M.R. Drinkwater, and A. Stoffelen, The Advanced scatterometer (ASCAT) on the meteorological operational (MetOp) platform: A follow on for the European wind scatterometers, Can. J. Remote Sensing ***28*** *(3)*, pp. 404-412, 2002.

[HERSBACH 2007] Hersbach, H., A. Stoffelen, and S. de Haan , An improved C-band scatterometer ocean geophysical model function: CMOD5, J. Geophys. Res., 112, C03006, 2007.

[PORTABELLA and STOFFELEN 2006] Marcos Portabella, Ad Stoffelen, Scatterometer backscatter uncertainty due to wind variability, IEEE Trans. Geosci. Rem. Sens. **44** (11), 3356-3362, 2006.

[PORTABELLA and STOFFELEN 2009] Portabella, M., and Stoffelen, A., "On scatterometer ocean stress," submitted to J. Atm. and Ocean Techn., 26 (2), pp. 368–382, 2009.

[STOFFELEN 1999] Stoffelen, Ad, "A Simple Method for Calibration of a Scatterometer over the Ocean", J. Atm. and Ocean Techn. 16(2), 275-282, 1999.

[STOFFELEN 1998] Stoffelen, Ad, "Scatterometry", KNMI*, PhD thesis at the University of Utrecht*, ISBN 90-39301708-9, October 1998

[STOFFELEN and ANDERSON 1997] Stoffelen, Ad, and David Anderson, "Scatterometer Data Interpretation: Measurement Space and inversion", J. Atm. and Ocean Techn., 14(6), 1298-1313, 1997.

[VERHOEF et al 2008] Verhoef, A., M. Portabella, A. Stoffelen and H. Hersbach, "CMOD5.n - the CMOD5 GMF for neutral winds", OSI SAF Technical Report SAF/OSI/CDOP/KNMI/TEC/TN/165, 2008

[VERSPEEK 2006] Verspeek, Jeroen, "Scatterometer calibration tool development", EUMETSAT Technical Report SAF/OSI/KNMI/TEC/RP/092, *KNMI*, de Bilt, 2006,

[VERSPEEK 2006-2] Verspeek, Jeroen, "User manual Measurement space visualisation package", *KNMI*, de Bilt, 2006

[VERSPEEK 2011] Verspeek, J., Verhoef, A and Stoffelen, A. "NWP ocean calibration", *KNMI*, de Bilt, 2011

[VERSPEEK 2011-2] Verspeek, A. and Stoffelen, A. "ASCAT GMF", DRAFT, *KNMI*, de Bilt, 2011